Cell Reports
Physical Science

CellPress
OPEN ACCESS

Article

Pump-valve dual-functional liquid metal soft actuators

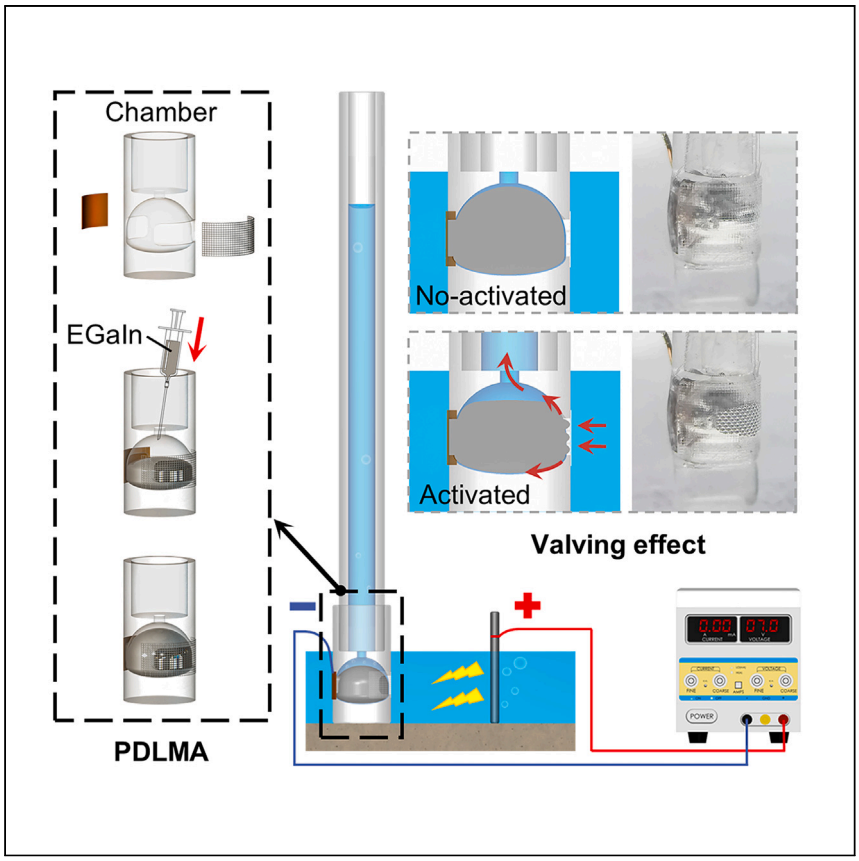

Ge et al. demonstrate a liquid-metal-enabled soft actuator that functions like a heart, with both pumping and valving functions but without any mechanical moving parts. It enables vertical pumping of various liquids, which is challenging to achieve using conventional micropumps. The actuator possesses the potential for constructing multifunctional devices for future soft robotics.

Du-An Ge, Erlong Wang, Shuai Dong, ..., Xiangpeng Li, Weihua Li, Shiwu Zhang

shiyang.tang@soton.ac.uk (S.-Y.T.)
licool@suda.edu.cn (X.L.)
swzhang@ustc.edu.cn (S.Z.)

Highlights

A liquid-metal-enabled pump-valve dual-functional actuator is proposed

The actuator achieves vertical pumping of liquid to a height exceeding 80 cm

The actuator can work with a diverse selection of liquids

The potential for contamination-free drug delivery is presented using the actuator

Ge et al., Cell Reports Physical Science 4, 101700
December 20, 2023
https://doi.org/10.1016/j.xcrp.2023.101700

Cell Reports
Physical Science

CellPress
OPEN ACCESS

Article

Pump-valve dual-functional liquid metal soft actuators

Du-An Ge,[1,5] Erlong Wang,[1,5] Shuai Dong,[1,5] Shiyuan Tong,[1] Mengli Sui,[1] Hongtai Ren,[1] Hu Jin,[1] Shi-Yang Tang,[2,*] Xiangpeng Li,[3,*] Weihua Li,[4] and Shiwu Zhang[1,6,*]

SUMMARY

Soft actuators offer several advantages over traditional rigid machines. Among soft materials, liquid metal (LM) is particularly noteworthy for its electro-responsive surface properties that induce flow or morphological changes, making it ideal for soft machines. Although using LM droplets as micropumps is simple, they face challenges in efficient vertical fluid pumping. Here, we report a pump-valve dual-functional LM soft actuator (PDLMA) that can continuously pump liquid upward. Benefiting from the unique conformability of LM, the PDLMA can provide the function of a check valve, which blocks the backflow of the rising liquid while continuing the pumping effect. At 6 V direct current (DC), the PDLMA lifts the solution more than 80 cm. We demonstrate the device's applications in circuit-on/off switches and pump-mixer systems. Moreover, as a conceptual experiment, we show the PDLMA's ability to achieve contamination-free drug delivery. The PDLMA represents a crucial step toward the development of soft actuators for flexible machines.

INTRODUCTION

As one of the most essential organs, the heart is the power source of the biological internal circulation system, and the heart valve can stop the return flow while continuously pumping blood.[1–4] There is an ever increasing interest in developing actuators that can simulate a heart, which plays a role as a highly effective fluid controller that has both pump and valve functions. In the past few decades, many such actuators have been developed, which can be divided into valved and valveless categories according to whether valving components are involved. A valved pump is generally operated by the periodic change of the cavity volume and the action of the one-way valve. Micropumps driven by piezoelectric,[5–8] electrostatic,[9–11] electrokinetic,[12–15] and hot-air brake[16] actuators belong to this category. Although the principle of the valved micropump is simple and the manufacturing process is mature, frequent switching of valve plates will lead to compromised reliability and reduced service life. Valveless micropumps use either asymmetric structures, such as diffusers and rotary plates,[17–21] instead of passive check valves or active electromechanical components to control the flow of fluids.[22] In addition, electrokinetic mechanisms such as electroosmotics[23–27] and potential gradient-induced Marangoni effect on liquid metal (LM)[28–32] can be used to pump liquid without using valves. However, the applications of these micropumps are hampered by limitations such as high operating voltage, limited working fluids, low flow rate, and low back pressure. The low back pressure makes achieving effective vertical pumping difficult for existing micropumps.

[1]CAS Key Laboratory of Mechanical Behavior and Design of Materials, Department of Precision Machinery and Precision Instrumentation, University of Science and Technology of China, Hefei, Anhui 230026, China

[2]School of Electronics and Computer Science, University of Southampton, Southampton, SO17 1BJ, UK

[3]College of Mechanical and Electrical Engineering, Soochow University, Suzhou 215000, China

[4]School of Mechanical, Materials, Mechatronic and Biomedical Engineering, University of Wollongong, Wollongong, Australia

[5]These authors contributed equally

[6]Lead contact

*Correspondence: shiyang.tang@soton.ac.uk (S.-Y.T.), licool@suda.edu.cn (X.L.), swzhang@ustc.edu.cn (S.Z.)

https://doi.org/10.1016/j.xcrp.2023.101700

As a well-known LM, mercury is difficult to popularize because of the extreme toxicity of its vapor.[33–35] In contrast, gallium (Ga)-based alloys such as EGaIn (75 wt % Ga and 25 wt % indium) and Galinstan (68.5 wt % Ga, 21.5 wt % indium, and 10 wt % tin) are promising materials for their low toxicity and near-zero vapor pressure.[36–39] Besides, these LMs have many excellent properties, such as high electrical and thermal conductivities, near-water viscosity, readily tunable interfacial tension, and good biocompatibility.[40–44] These properties have enabled the use of LM in many areas, such as wearable electronic devices,[45–51] reconfigurable radiofrequency (RF) devices,[52,53] and artificial muscles.[54,55] Additionally, the Marangoni flow effect induced by LM has been reported in many studies related to robotic actuation.[56–58] Once a difference in surface tension along the LM droplet exists (induced by an electric field[59] or chemical reaction[60]), the droplet generates Marangoni flows that pulls liquids from regions with lower interfacial tension toward areas with higher tension along the surface. This actuation method exhibits low power consumption and eliminates the need for rigid connecting components, rendering it a promising candidate for integration within fully flexible actuation systems.

In this study, we draw inspiration from the heart's valving mechanism for unidirectional flow and use the Marangoni effect induced by LM. Leveraging the conformability of LM, the pump-valve dual-functional LM soft actuator (PDLMA) we describe provides a check valve function that blocks backflow while continuing to pump the liquid. We verify the existence of the induced upward flow and optimize the structure of the PDLMA by both simulation and experiments. More important, multiple PDLMAs can be reconfigured in parallel or in series to offer enhanced pumping performance. Additional experiments are performed to explore the potential of PDLMA in applications of circuit switches and liquid agitations. Finally, to highlight the potential of PDLMA for biomedical applications, we operate the PDLMA to drive air embolism for transporting liquid drugs, demonstrating its capability for contamination-free drug delivery. In Table S1, we compare our work with existing prototypes, including some commercial products, across various performance metrics, demonstrating the structural advantages of our integrated pump-valve design and its excellent performance in vertical pumping with low power consumption.

RESULTS AND DISCUSSION

Operating principle of the PDLMA

Figure 1A shows the schematic of a PDLMA. The PDLMA consists of four major parts: a three-dimensional (3D)-printed pump chamber, a copper electrode flake with wire, filter gauze, and an EGaIn LM droplet, as shown in Figure 1B. The role of each part is elaborated below.

LM droplet

In this study, EGaIn LM is used as the core of the PDLMA to induce vertical pumping of the surrounding liquids.

Chamber

The 3D-printed chamber made of transparent photosensitive resin is specially designed to hold the LM droplet, and it is plasma-treated to improve its surface hydrophilicity to prevent the accumulation of gas bubbles (see Figure S1 in the supplemental information for details). We adopt a vertical looped quartz tube as the conduit for elongating the pump's outlet. When the LM droplet is activated, the structure of the chamber can facilitate Marangoni flow induced by the surface tension gradient across the LM droplet to flow upward.

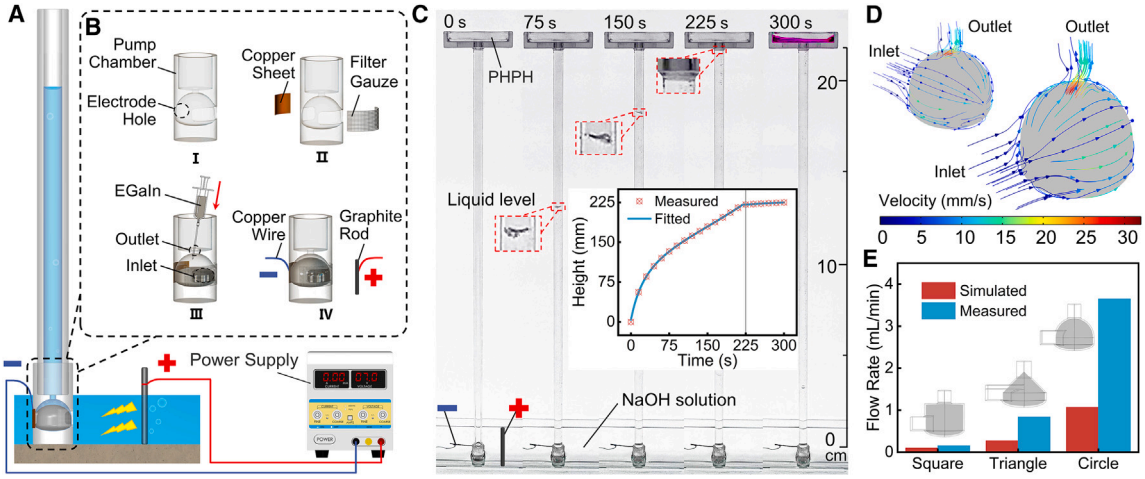

Figure 1. Structure and operation of the PDLMA

(A and B) (A) Schematics and (B) assembly process of a PDLMA unit.

(C) Pumping 0.5 mol/L NaOH solution upward using a PDLMA. The inset is the height-vs.-time plot of the pumped NaOH solution.

(D) CFD simulation of the flow velocity vectors (millimeters per second) along the LM droplet surface.

(E) Simulated and measured flow rates for different section shapes of the holder.

Electrode

We exploit the excellent wetting performance between Cu and LM to anchor the LM droplet onto a Cu sheet. We connect the Cu sheet to the negative pole of the direct current (DC) power supply; therefore, the LM droplet can be continuously reduced to remove the oxide layer on its surface and generate Marangoni flows. In our study, the PDLMA is found to be able to continuously pump liquid even after operating for more than 8 h, with no observed oxide layer on the surface of the droplet. The theoretical lifetime of a PDLMA is >800 days (see supplemental experimental procedures). A graphite rod is used as an inert electrode, and it is connected to the positive pole of the DC power supply.

Filter gauze

A strip of fine and closely woven filter gauze, made of polyamide, is attached to the pump chamber's inlet. The filter gauze is plasma treated to improve its surface hydrophilicity (see Figure S1). The filter gauze not only prevents the LM droplet from escaping but also endows the valving effect to avoid the backflow of pumped liquid caused by gravity.

To characterize the upward pumping effect, we embed and fix a quartz tube in the pipe joint at the top of the pump chamber so that the liquid level can be monitored. Phenolphthalein (PHPH), a chemical that can change its color to purple when mixed with a basic liquid, is added to the container on top of the quartz tube to show the existence of NaOH solution after pumping. Figure 1C shows sequential snapshots of the vertical pumping effect induced by the PDLMA under 6 V activation (see Video S1 in the supplemental information), in which we can see the rising of the concave meniscus in the tube over time, and the color of liquid changes to purple when reaching the container located ~22 cm above the PDLMA. The time-vs.-height plot in the inset of Figure 1C indicates that the rising speed of the liquid level attenuates within the first minute of pumping and then becomes constant. When the PDLMA is activated, the EGaIn droplet deforms and is squeezed against the filter gauze by back pressure. As the liquid level rises, the back pressure also increases to induce more deformation on the LM droplet, making it block the filter further to reduce the amount of inflow.

We next conduct computational fluid dynamics (CFD) numerical simulations to optimize the structure of the PDLMA. To induce the Marangoni effect, an external electrical potential gradient is applied along the LM droplet surface, which leads to a surface tension gradient. The relationship of surface tension γ and the potential across the electrical double layer V is described by Lippman's equation:

$$\gamma = \gamma_0 - \frac{1}{2}CV^2. \quad \text{(Equation 1)}$$

On the basis of our previous work[61] and inspired by the operation of the valve in the heart, we design and optimize the pump chamber in order to achieve the best pumping performance.

We conduct CFD simulations to verify the flow field on the surface of the LM droplet during pumping. To do so, we apply an electrical potential drop across the LM droplet to generate a surface tension gradient. A flow of fluid is induced by the surface tension gradient and the resulting flow field is guided upward confined by the internal structure of the chamber, as shown in Figure 1D. The structure of the chamber is critical for affecting the pumping performance.[61] We conduct a series of experiments and simulations using chambers of different cross-sectional shapes, including square, triangle, and circle, as shown in Figure 1E (see Figure S2 for detailed flow fields). We aim to use simulations to guide the design of the pump chamber structure. In comparison with experimental data, our simulation results consistently exhibited trends in flow rate variations for different chamber shapes, with predicted flow rates falling within the same order of magnitude. The discrepancies between the simulated and actual results stem from the inability to accurately model the intricate morphological changes of the LM droplet, which result from the interplay of liquid-liquid, solid-liquid, and external potential gradients. Both simulations and experiments indicate that the circular shaped chamber offers the optimum performance. We further investigate the effects of other parameters such as inlet area, outlet area, the volume of the LM droplet, and applied voltage on the pumping performance using simulations, as detailed in Figure S3. In general, a larger inlet/outlet area and applied voltage can lead to higher flow rates, while the size of the LM droplet should not be too large to cause blockage of the channel.

The valving function of the PDLMA

The LM droplet in the chamber can also act as a valve. When voltage is applied, the LM droplet is activated and the Marangoni flow pumps the surrounding liquid to cause the liquid column to rise. As pumping continues, the height of the liquid column steadily increases and generates higher back pressure on the LM droplet, forcing the LM droplet to deform and squeezing it toward the filter gauze. This results in the blockage of the flow and the reduction in the flow speed (Figure 2A). It should be noted that, without the constrain of the chamber, the Marangoni effect can only produce a localized flow field around the LM droplet without the ability to bring the electrolyte upward. Therefore, the deformed LM droplet acts as a pump and a valve simultaneously to induce a unidirectional flow of liquid. Figure 2B demonstrates the synergistic pumping-valving effect. We inject EGaIn into the chamber until it overflows into the quartz pipe and add NaOH solution into the pipe. Upon activating the PDLMA, the level of the liquid rises because of the pumping effect. When deactivating the PDLMA, the level of the liquid remains unchanged, indicating the valving effect induced by the LM droplet.

In order to verify that the continuous rise of the liquid level in the quartz pipe is attributed mainly to the unidirectional valving effect of the LM droplet, we conduct an

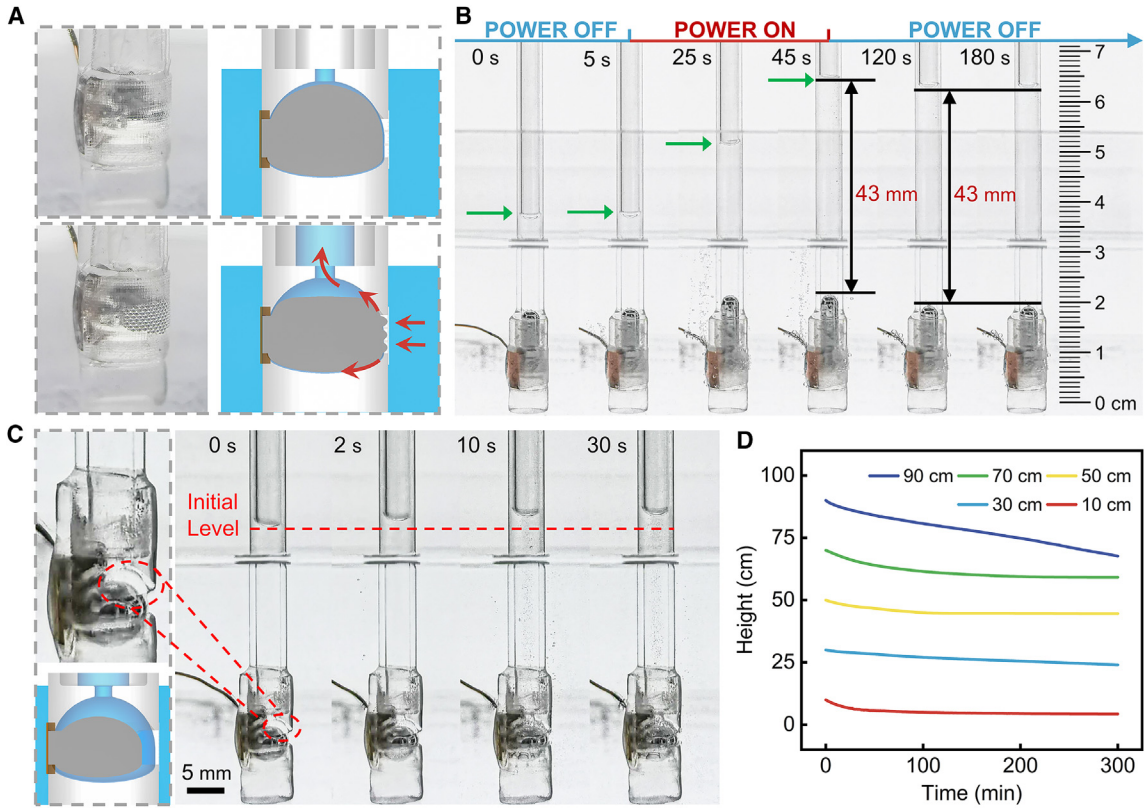

Figure 2. Valving effect of the PDLMA

(A) Illustrations and photographs of the PDLMA when activated.

(B) Valving effect induced by the LM droplet after deactivating the PDLMA.

(C) Smaller LM droplet without the ability to induce the valving effect fail to pump liquid upward.

(D) Height-vs.-time plot with different heights of initial liquid level.

experiment using an EGaIn droplet of smaller size, so that it cannot touch the filter gauze to block the flow of liquid, as shown in Figure 2C. We observe only ~1 mm of liquid rise after activating the droplet for 30 s, indicating that the size of the LM droplet needs to be sufficiently large in order to function as a valve, thereby enabling the vertical pumping of liquid.

We further examine the effectivity of the valving effect by injecting liquid of various heights (10–90 cm) into the quartz pipe and observing the change of liquid level over time, as shown in Figure 2D. Without activating the PDLMA, we can see a more obvious reduction in the liquid level over time for both low (10 cm) and high (>75 cm) initial liquid level conditions. This is because a low liquid level generates less back pressure to deform the LM droplet to seal the filter gauze, while the large back pressure induced by a high liquid level significantly deforms the droplet and even causes leakage of LM.

Investigating factors affecting pumping performance

We next investigate a series of parameters that may affect the performance of the PDLMA, including the mesh size of the filter gauze, operating voltage, the size of the LM droplet, the concentration of NaOH, and the size of the outlet aperture. Figure 3A shows that increasing the filter mesh number leads to a higher liquid level after activating the PDLMA, where the flow rate is not significantly compromised. As

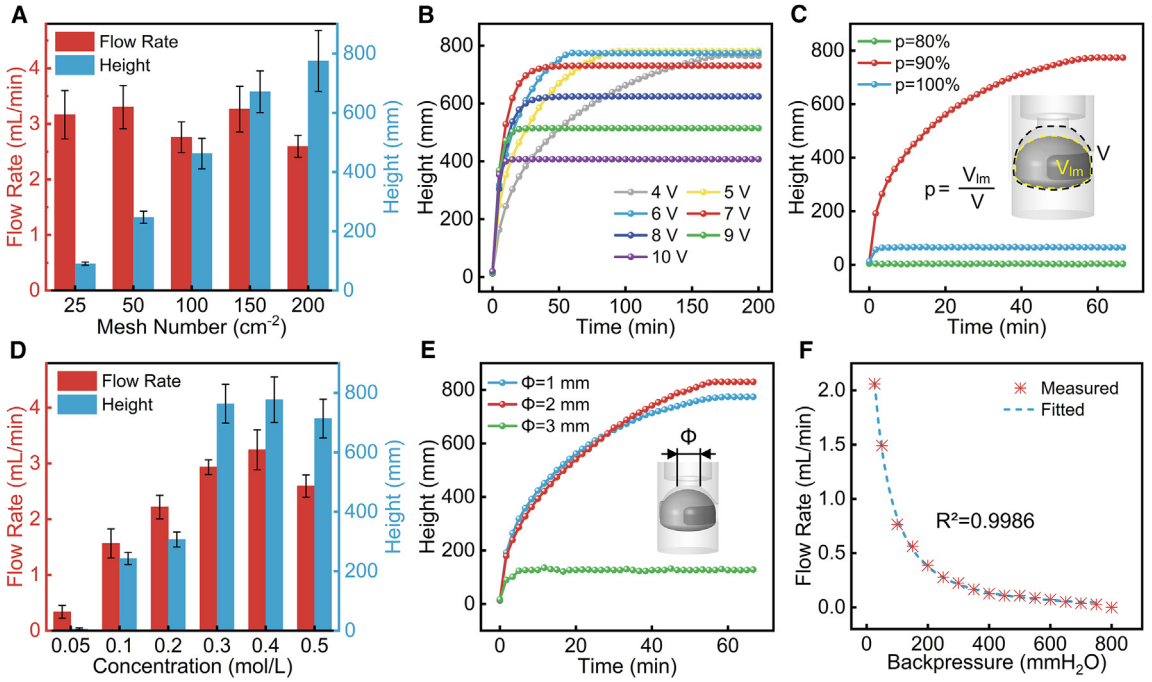

Figure 3. Parameters affecting the pumping performance of the PDLMA

(A) Changes in the flow rate and height with respect to mesh number. Error bars represent standard deviation ($n \geq 5$).

(B and C) Change in liquid level with respect to time under different (B) voltages and (C) LM volumes.

(D) Changes in the flow rate and height with respect to NaOH concentration. Error bars represent standard deviation ($n \geq 5$).

(E) Changes in liquid level with respect to time under different outlet aperture sizes.

(F) Flow rate vs. back pressure plot for the case with 1 mm outlet aperture.

discussed in the previous section, a denser mesh enhances the valving effect to prevent the backflow of pumped liquid and leakage of LM. A larger external potential can generate a steeper surface tension gradient along the surface of the LM droplet, thereby leading to a higher flow rate to make the pumped liquid reach the equilibrium position earlier, as shown in Figure 3B. However, if the applied voltage is larger than 7 V, the maximum liquid level decreases, which is due to the blockage of the channel induced by the gas bubbles generated by electrolysis.

Our CFD simulations reveal that the size of the LM droplet affects the pumping performance (see Figure S3 in the supplemental information for details). This is also verified by our experimental results, as shown in Figure 3C. The PDLMA cannot pump vertically when the LM droplet takes less than 80% of the chamber volume, and increasing the volume percentage p to 90% leads to a significant improvement of the pumping performance. This can be explained by the necessary valving effect, which requires the LM droplet to be sufficiently large to block the backflow of the pumped liquid. However, an oversized LM droplet will also block the upward flow of liquid to compromise the pumping effect (see the p = 100% case in Figure 3C). Our simulations are incapable of predicting the case with oversized LM droplets, which is because our model cannot reflect the deformation of the LM droplet during pumping. The PDLMA is capable of working in NaOH solutions with a wide range of concentrations. In Figure 3D, increasing the NaOH concentration from 0.05 to ~0.4 mol/L results in better pumping performance. However, this also leads to a higher production of gas bubbles on the LM droplet, as shown in Figure S4. Some of these bubbles escape through the filter at the inlet, obstructing the flow of the electrolyte into the chamber and reducing the pumping speed. In comparison with lower

concentration scenarios, the LM droplet becomes more susceptible to leakage through the filter at identical back pressure, disrupting the valve function and reducing the maximum achievable pumping height.

As predicted by our simulation results given in Figure S3, our experiments verify that the outlet aperture of the chamber also affects the pumping performance, as shown in Figure 3E. The PDLMA works effectively with aperture diameters of 1 and 2 mm; however, increasing the aperture to 3 mm deteriorates the pumping effect. This is because the larger outlet cannot effectively restrict the escape of the EGaIn droplet during pumping. Upon the application of voltage, the LM droplet tends to move toward the graphite rod (the positive electrode of the power supply), resulting in its emergence from the outlet, which is not accounted for in the CFD model. This phenomenon also obstructs the rising channel of the electrolyte, thereby affecting the pump's functionality. The final height of the liquid column is 775 mm when the outlet diameter measures 1 mm and increases to 830 mm when the diameter is 2 mm. It is remarkable that such significant final heights can be achieved given that the PDLMA itself is only about 10 mm in size. Although the 1 mm outlet aperture performs better than the 2 mm one in terms of final liquid column pumping height, it has a higher pumping rate. From our experimental observation, a 1 or 2 mm aperture provides a better ability to withstand back pressure from the liquid in the tube, leading to a better valving effect thereby the pumping performance. We select the case when the outlet aperture is 1 mm and plot the corresponding pressure-flow curve to reflect the pumping characteristics of the PDLMA, as shown in Figure 3F. We further examine the pumping performance with different electrolyte solutions and inner diameters of quartz tubes, as detailed in Figure S5. Benefiting from directly using the LM droplet as the cathode, the PDLMA effectively operates with a diverse range of electrolytes, displaying minimal variations in performance. In addition, the final heights of the liquid level are almost the same for tubes with diameters from 3 to 7 mm. A larger tube diameter reduces the liquid rising velocity but not the final height.

Applications of the PDLMA

The simple structure and operation of the PDLMA make it possible to reconfigure multiple actuators to enhance performance. Inspired by electrical circuits where a series connection of power supplies provides higher voltage output and a parallel connection offers larger current, multiple PDLMA can be reconfigured in series or parallel to improve the flow rate or the height of liquid level. Figure 4A shows the monitored flow rate for a system with four PDLMA connected in series. A reservoir platform is used to connect two PDLMA units in series in the vertical direction. This structure resets the back pressure so that when the solution flows through the next actuator, the original peak flow rate can be reached again (Figure 4A). As a result, the high flow rate can be maintained without decreasing when the liquid level is high. The flow rate of a single PDLMA decreases from 3,700 to 1,700 μL/min within 7 s, the activation of the PDLMA in the next stage restores the flow rate, allowing for rapid pumping of liquid to a higher level compared with a single PDLMA. In the parallel configuration given in Figure 4B, four PDLMA units result in a high output volume of 3,223 μL within 40 s, which is about four times the output volume achieved when a single unit is used.

We further explore the hybrid configuration connecting PDLMA units in both series and parallel, as shown in Figure 4C. This system has a three-level tower pipeline network composed of PDLMA units (see also Figure S6 in the supplemental information for details). The first level consists of four units connected in parallel, and the

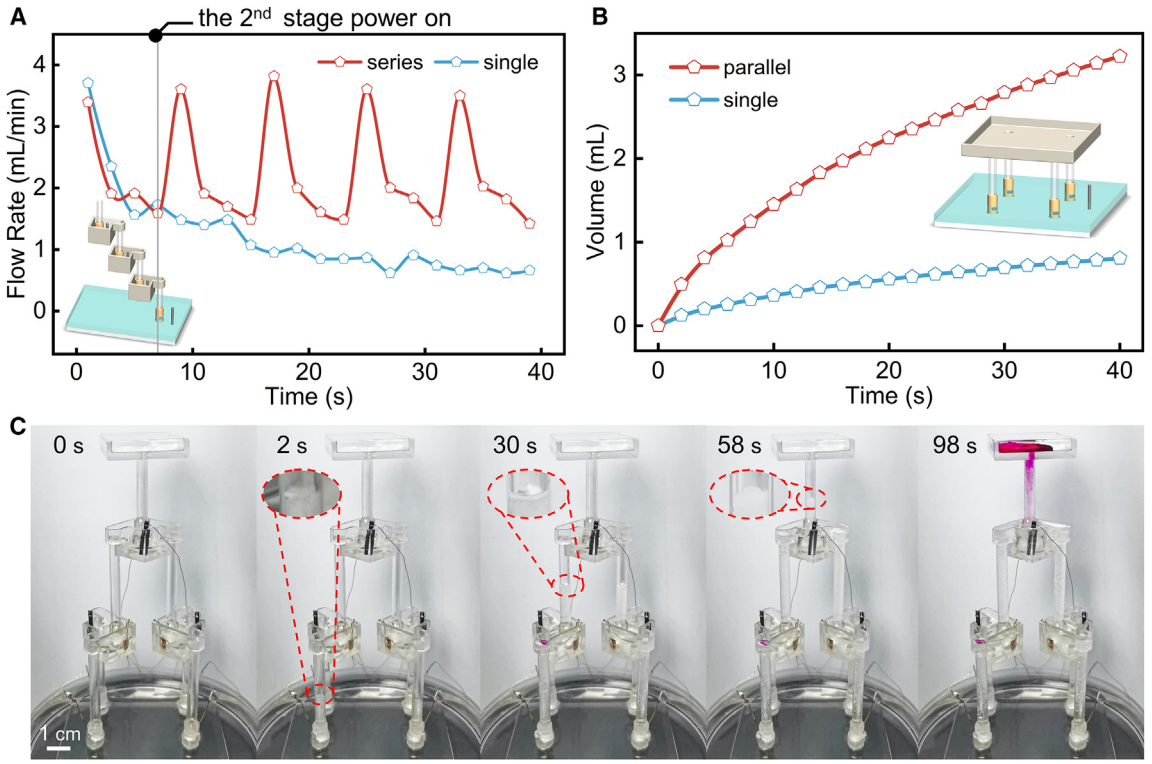

Figure 4. Parallel and series configurations of the PDLMA

(A) Change in flow rate with respect to time with a single PDLMA and four PDLMA units connected in series. The inset shows the experimental setup.

(B) Change in pumped liquid volume with respect to time with single PDLMA and four PDLMA units connected in parallel.

(C) A vertical pumping system with PDLMA units connected in both series and parallel pumps NaOH solution vertically into a container with PHPH (100 mesh number cm^{-2}, 6 V DC, 0.5 mol/L NaOH solution, LM droplet/chamber volume ratio 90%, diameter of outlet aperture 1 mm).

second level has two PDLMA units connected in parallel that are in series with the first level. The third level has one PDLMA and the top has a container filled with PHPH. Each level is integrated with an independent switch to control the on-off state of the PDLMA units. When PDLMA units in each level are activated sequentially, liquid can be pumped upward from the lower level to the container on the top within 100 s (see also Video S2 in the supplemental information).

Harnessing the versatility of the PDLMA, we further investigate its applications in controlling circuits, mixing liquids, and building contamination-free liquid drug infusion devices. Figure 5A demonstrates the use of a PDLMA as a switching circuit for activating LED lights. With the increase in the NaOH solution level, the conductive electrolyte connects the circuit in a sequence to turn on light-emitting diodes (LEDs) with the shape of "USTC" (see also Video S3 in the supplemental information). As the PDLMA can be connected in series or parallel, we demonstrate the mixing and vertical transportation of two different liquids from separated reservoirs, as shown in Figure 5B. We fill two Petri dishes with blue and yellow colored NaOH solution (0.5 mol/L) and used three PDLMA units to first mix the liquid from the two reservoirs and pump the mixed liquid toward the container on the top. The chaotic advection generated by the Marangoni flow can efficiently mix the two incoming liquids and meanwhile pump the mixed fluid toward the top reservoir (see also Video S4 in the supplemental information).

Finally, we design a contamination-free liquid drug infusion device using an air embolism in the infusion pipe to separate the working solution (NaOH solution) and

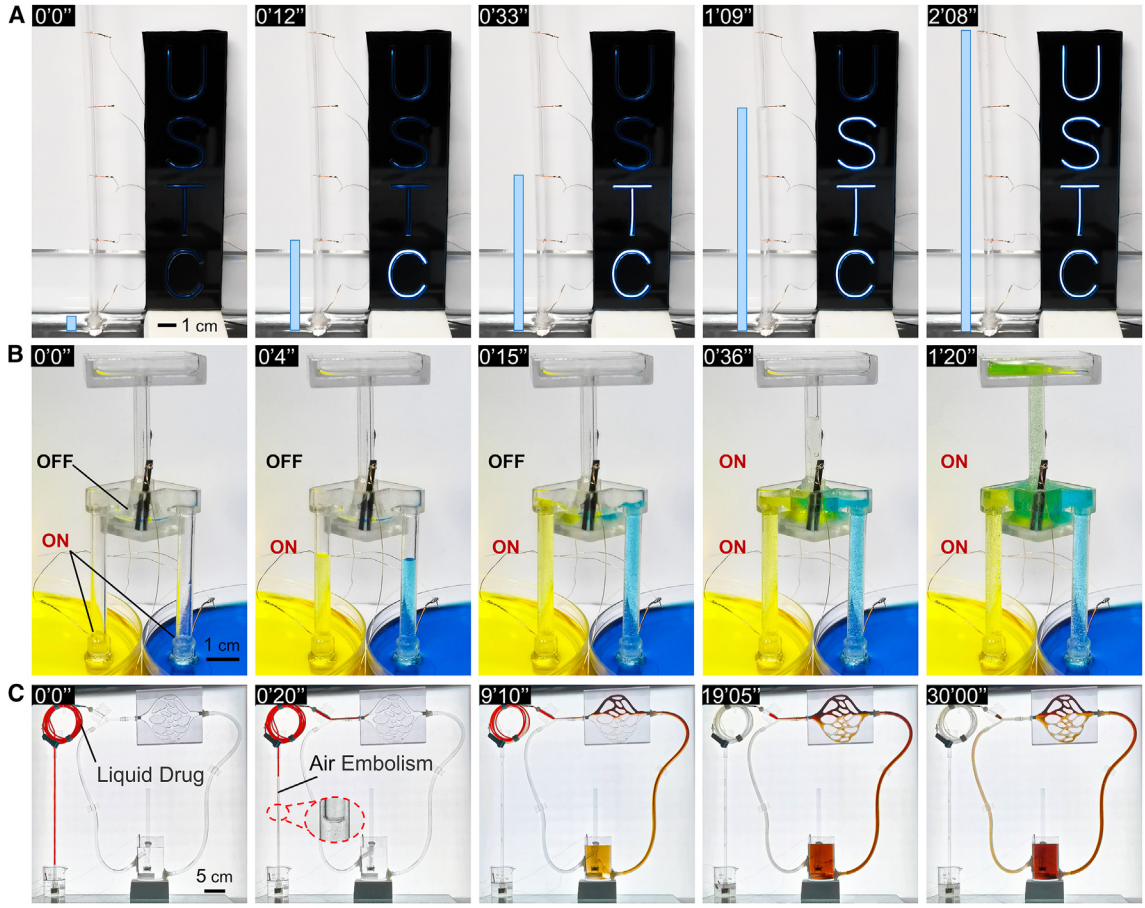

Figure 5. Examples of applications of the PDLMA

(A) Sequential snapshots showing a circuit-on/off switch on the basis of the PDLMA.

(B) Sequential snapshots showing a pump-mixer system enabled by the PDLMA.

(C) Sequential snapshots showing a contamination-free liquid drug infusion device on the basis of the PDLMA (150 mesh number cm^{-2}, 6 V DC, 0.5 mol/L NaOH solution, LM droplet/chamber volume ratio 90%, diameter of outlet aperture 2 mm).

schematic liquid drug (deionized water dyed with red ink). As depicted in Figure 5C, we assemble a conceptual biological internal circulation system where the PDLMA plays the role of a heart in the system. On the left of the internal circulation system is the infusion part which is driven by a PDLMA. We inject 20 mL of liquid drug colored with red dye into the pipe in advance, one end of the pipe is connected to the internal circulation system, and a section of air is reserved at the other end to isolate the drug from the NaOH solution used for pumping. Upon activating the PDLMA, NaOH solution is pumped to push the air embolism in the pipe, resulting in the infusion of the liquid drug into the internal circulation system without contamination (see Video S5 in the supplemental information). The produced hydrogen gas bubbles in the PDLMA eventually merge with the initially reserved air embolism, which contributes to the growth of the air embolism to provide better isolation. We cut off the power of the contamination-free liquid drug infusion device by removing the graphite electrode about 19 min after the injection start, while keeping the power supply of the internal circulation system. After 54 min, the liquid drug in the internal circulation system is uniformly dispersed under the continuous pumping of the heart organ played by the PDLMA (see Figure S7 in the supplemental information for details).

In summary, by using an EGaIn droplet as the core, we propose a soft actuator that functions as both a pump and a valve. Without mechanical moving parts, the PDLMA is easy to fabricate, operate, and maintain, offering excellent maneuverability and reconfigurability. When a DC voltage is applied to the EGaIn droplet, the PDLMA's chamber structure guides the flow generated by the Marangoni effect to move vertically through the outlet. Meanwhile, the valving effect is generated between the EGaIn droplet and the filter screen, intercepting the backflow during vertical pumping. With just 100 μL EGaIn and a 6 V DC input, the device can raise the electrolyte more than 80 cm and reach a high initial flow rate of 3,600 μL/min. We thoroughly investigate the PDLMA's operating parameters and structural design to optimize its performance. Assembling multiple PDLMA units in parallel and in series can improve the flow rate and height limit of the liquid level. The PDLMA's dual functionality as a pump and valve under low driving voltage has enormous potential in constructing multifunctional devices, including circuit-on/off switches, integrated pump-mixer systems, and contamination-free liquid drug infusion devices. We believe that the PDLMA will offer new opportunities for developing future soft robotics and electronics.

EXPERIMENTAL PROCEDURES

Resource availability

Lead contact

Further information and requests for resources and reagents should be directed to and will be fulfilled by the Lead Contact, Shiwu Zhang (swzhang@ustc.edu.cn).

Materials availability

This study did not generate new unique materials.

Data and code availability

The data generated in this study are available from the lead contact upon reasonable request.

Materials

EGaIn was purchased from Santech Materials Co., Ltd. The Cu sheets and wires were purchased from Yuandelai Industrial Materials Co., Ltd. NaOH was purchased from Aladdin. The pump chambers were 3D-printed from transparent photosensitive resin (Form 2; Formlabs), and the assembled units were modified by air plasma cleaner (VP-R5; SUNJUNE) to make surface of inner pump chamber hydrophilic. Quartz pipes were purchased from Donghua Quartz Products Co., Ltd. The DC voltage was provided by a DC power supply (DP832; RIGOL). Most bonding was achieved with chemically inert UV curing adhesive (LEAFTOP).

Experimental design

The PDLMA chamber, optimized beforehand through simulations, was 3D-printed and treated with a plasma cleaner to make its surface hydrophilic. Afterward, we installed a copper plate and a filter onto the pump chamber and used photosensitive resin as an adhesive to secure them in place. Then, we extracted an appropriate amount of EGaIn with a syringe and injected it into the PDLMA chamber, ensuring the LM droplet makes good contact with and wets the copper plate. The assembled PDLMA unit was submerged in NaOH solution (usually 0.5 mol/L) and all the air in the PDLMA chamber was evacuated. Next, the negative pole of a DC power source was connected to the copper plate to maintain the LM droplet in an electrochemical reduction state during the experiment and prevented it from losing its surface mobility because of oxidation. The positive pole of the power source was linked to a 2 mm diameter graphite rod, which was inserted into the NaOH solution and positioned 5 cm from the PDLMA inlet.

Most experiments were conducted under a 6 V applied voltage. A quartz pipe, 1 m in length, was attached to the PDLMA outlet. We embedded a vertical quartz pipe into an acrylic board with a red LED strip, placed directly behind the quartz pipe. When the LED strip was illuminated, the refraction effect of the light clearly marked the liquid column height, allowing the industrial camera to capture the liquid surface position easily. Finally, the liquid surface height data were obtained by processing the video frame by frame to identify the liquid surface position.

CFD simulation

The numerical simulations were conducted using COMSOL, where the models were constructed using the electric currents and creeping flow modules. The Marangoni phenomenon, which causes fluid flow, occurs when a tension gradient exists in the two-phase interface. By applying an electric field, we can alter the potential distribution of the droplet surface and generate a tension gradient. The potential difference across the droplet and the surface tension between the LM and electrolyte follow Lippman's equation (Equation 1). The governing equations that the fluid in the device satisfies are as follows.

Electric field governing equations

$$\nabla \cdot \vec{J} = 0 \quad \text{(Equation 2)}$$

$$\vec{J} = \sigma \vec{E} \quad \text{(Equation 3)}$$

and

$$\vec{E} = -\nabla V \quad \text{(Equation 4)}$$

Where σ is the conductivity of electrolyte, $\vec{J}$ is the current density, $\vec{E}$ is the electric field intensity, and V is the voltage.

Flow field governing equations

The fluid satisfies the Navier-Stokes equation and incompressible fluid continuity equation and consider steady flow:

$$\rho(\vec{u} \cdot \nabla \vec{u}) = \nabla \cdot [-pI + K] + \vec{F} \quad \text{(Equation 5)}$$

$$K = \mu\left[\nabla \vec{u} + (\nabla \vec{u})^T\right] \quad \text{(Equation 6)}$$

and

$$\nabla \cdot \vec{u} = 0 \quad \text{(Equation 7)}$$

Stress conditions on liquid metal surface

$$[-pI + K]\vec{n} = \nabla_\tau \gamma \quad \text{(Equation 8)}$$

Where I is the identity matrix, K is the shear stress matrix, $\vec{u}$ is fluid velocity, ρ is fluid density, p is pressure, μ is viscosity, $\vec{F}$ is external force per unit volume fluid received, and $\vec{n}$ is the unit vector that is normal to the surface.

SUPPLEMENTAL INFORMATION

Supplemental information can be found online at https://doi.org/10.1016/j.xcrp.2023.101700.

ACKNOWLEDGMENTS

This work was supported in part by grants from the National Natural Science Foundation of China (grants 51975550 and U21A20119) and a grant from Major Science and Technology Projects in Anhui Province (grant 202203a07020016). X.L. is supported by a grant from the Natural Science Found for Colleges and Universities of Jiangsu Province (grant 22KJA510006) and S.-Y.T. is supported by a grant from the Engineering and Physical Sciences Research Council (EPSRC) (grant EP/V008382/1). H.J. is supported by the Natural Science Foundation of Anhui Province of China (grant 2008085UD02).

AUTHOR CONTRIBUTIONS

D.-A.G., E.W., and S.Z. conceptualized and designed the research. D.-A.G. and E.W. conducted the experiments and wrote the original draft. S.T. and H.R. helped with the CFD simulations. S.D. and M.S. provided assistance on the figures. S.-Y.T. reviewed and edited the manuscript. H.J., W.L., S.-Y.T., and X.L. supervised the work.

DECLARATION OF INTERESTS

The authors declare no competing interests.

Received: July 24, 2023
Revised: October 17, 2023
Accepted: November 2, 2023
Published: November 22, 2023

REFERENCES

1. Mol, A., Rutten, M.C.M., Driessen, N.J.B., Bouten, C.V.C., Zünd, G., Baaijens, F.P.T., and Hoerstrup, S.P. (2006). Autologous human tissue-engineered heart valves: prospects for systemic application. Circulation *114*, I152–I158.

2. Sotiropoulos, F., Le, T.B., and Gilmanov, A. (2016). Fluid Mechanics of Heart Valves and Their Replacements. Annu. Rev. Fluid Mech. *48*, 259–283.

3. Catterall, F., Ames, P.R., and Isles, C. (2020). Warfarin in patients with mechanical heart valves. BMJ Br. Med. J. (Clin. Res. Ed.) *371*, m3956.

4. Fioretta, E.S., Motta, S.E., Lintas, V., Loerakker, S., Parker, K.K., Baaijens, F.P.T., Falk, V., Hoerstrup, S.P., and Emmert, M.Y. (2021). Next-generation tissue-engineered heart valves with repair, remodelling and regeneration capacity. Nat. Rev. Cardiol. *18*, 92–116.

5. Ude, C., Hentrop, T., Lindner, P., Lücking, T.H., Scheper, T., and Beutel, S. (2015). New perspectives in shake flask pH control using a 3D-printed control unit based on pH online measurement. Sens. Actuator B-Chem *221*, 1035–1043.

6. Lee, J., Wipf, M., Mu, L., Adams, C., Hannant, J., and Reed, M.A. (2017). Metal-coated microfluidic channels: An approach to eliminate streaming potential effects in nano biosensors. Biosens. Bioelectron. *87*, 447–452.

7. Esplandiu, M.J., Reguera, D., Romero-Guzmán, D., Gallardo-Moreno, A.M., and Fraxedas, J. (2022). From radial to unidirectional water pumping in zeta-potential modulated Nafion nanostructures. Nat. Commun. *13*, 2812.

8. Shouji, Y., Sekine, T., Ito, K., Ito, N., Yasuda, T., Wang, Y.F., Takeda, Y., Kumaki, D., Santos, F.D.D., Miyabo, A., and Tokito, S. (2023). Fast Response, High-Power Tunable Ultrathin Soft Actuator by Functional Piezoelectric Material Composite for Haptic Device Application. Adv. Electron. Mater. *9*, 2201040.

9. Nisar, A., Afzulpurkar, N., Mahaisavariya, B., and Tuantranont, A. (2008). MEMS-based micropumps in drug delivery and biomedical applications. Sens. Actuator B-Chem. *130*, 917–942.

10. Afshar Farniya, A., Esplandiu, M.J., Reguera, D., and Bachtold, A. (2013). Imaging the proton concentration and mapping the spatial distribution of the electric field of catalytic micropumps. Phys. Rev. Lett. *111*, 168301.

11. Lee, K.K., and Ahn, C.H. (2013). Superhydrophilic multilayer silica nanoparticle networks on a polymer microchannel using a spray layer-by-layer nanoassembly method. ACS Appl. Mater. Interfaces *5*, 8523–8530.

12. Reichmuth, D.S., Chirica, G.S., and Kirby, B.J. (2003). Increasing the performance of high-pressure, high-efficiency electrokinetic micropumps using zwitterionic solute additives. Sens. Actuator B-Chem. *92*, 37–43.

13. Paxton, W.F., Baker, P.T., Kline, T.R., Wang, Y., Mallouk, T.E., and Sen, A. (2006). Catalytically induced electrokinetics for motors and micropumps. J. Am. Chem. Soc. *128*, 14881–14888.

14. Feng, H., Chang, H., Zhong, X., and Wong, T.N. (2020). Recent advancement in induced-charge electrokinetic phenomena and their micro- and nano-fluidic applications. Adv. Colloid Interface Sci. *280*, 102159.

15. Weiß, L.J.K., Music, E., Rinklin, P., Banzet, M., Mayer, D., and Wolfrum, B. (2022). On-Chip Electrokinetic Micropumping for Nanoparticle Impact Electrochemistry. Anal. Chem. *94*, 11600–11609.

16. Kim, J.-H., Na, K.-H., Kang, C.J., and Kim, Y.-S. (2005). A disposable thermopneumatic-actuated micropump stacked with PDMS layers and ITO-coated glass. Sens. Actuator A-Phys. *120*, 365–369.

17. Zhang, T., and Wang, Q.-M. (2006). Performance of miniaturized direct methanol fuel cell (DMFC) devices using micropump for fuel delivery. J. Power Sources *158*, 169–176.

18. Chuech, S.G., Chen, C.-C., Lu, J.-C., and Yan, M.-M. (2007). Design and implementation of ejector driven micropump. Energy Convers. Manag. *48*, 2657–2662.

19. Fleischmann, E.K., Liang, H.L., Kapernaum, N., Giesselmann, F., Lagerwall, J., and Zentel, R. (2012). One-piece micropumps from liquid crystalline core-shell particles. Nat. Commun. *3*, 1178.

20. Heo, H.Y., Chung, S., Kim, Y.T., Kim, D.H., and Seo, T.S. (2016). A valveless rotary microfluidic device for multiplex point mutation identification based on ligation-rolling circle

amplification. Biosens. Bioelectron. *78*, 140–146.

21. Thomas, D.J., Tehrani, Z., and Redfearn, B. (2016). 3-D printed composite microfluidic pump for wearable biomedical applications. Addit. Manuf. *9*, 30–38.

22. Choi, G., Fitriasari, E.I., and Park, C. (2021). Electro-Mechanochemical Gating of a Metal-Phenolic Nanocage for Controlled Guest-Release Self-Powered Patches and Injectable Gels. ACS Nano *15*, 14580–14586.

23. Miao, J.Y., Xu, Z.L., Zhang, X.Y., Wang, N., Yang, Z.Y., and Sheng, P. (2007). Micropumps Based on the Enhanced Electroosmotic Effect of Aluminum Oxide Membranes. Adv. Mater. *19*, 4234–4237.

24. Wang, X., Wang, S., Gendhar, B., Cheng, C., Byun, C.K., Li, G., Zhao, M., and Liu, S. (2009). Electroosmotic pumps for microflow analysis. Trends Anal. Chem. *28*, 64–74.

25. Ai, Y., Yalcin, S.E., Gu, D., Baysal, O., Baumgart, H., Qian, S., and Beskok, A. (2010). A low-voltage nano-porous electroosmotic pump. J. Colloid Interface Sci. *350*, 465–470.

26. Jun, I.K., and Hess, H. (2010). A biomimetic, self-pumping membrane. Adv. Mater. *22*, 4823–4825.

27. Li, X., Liu, S., Fan, P., Werner, C.F., Miyamoto, K.-i., and Yoshinobu, T. (2017). A bubble-assisted electroosmotic micropump for a delivery of a droplet in a microfluidic channel combined with a light-addressable potentiometric sensor. Sens. Actuator B-Chem. *248*, 993–997.

28. Hutter, T., Bauer, W.-A.C., Elliott, S.R., and Huck, W.T.S. (2012). Formation of Spherical and Non-Spherical Eutectic Gallium-Indium Liquid-Metal Microdroplets in Microfluidic Channels at Room Temperature. Adv. Funct. Mater. *22*, 2624–2631.

29. Tang, S.Y., Khoshmanesh, K., Sivan, V., Petersen, P., O'Mullane, A.P., Abbott, D., Mitchell, A., and Kalantar-Zadeh, K. (2014). Liquid metal enabled pump. Proc. Natl. Acad. Sci. USA *111*, 3304–3309.

30. Zhang, J., Yao, Y., Sheng, L., and Liu, J. (2015). Self-fueled biomimetic liquid metal mollusk. Adv. Mater. *27*, 2648–2655.

31. Han, J., Mayyas, M., Tang, J., Mousavi, M., Idrus-Saidi, S.A., Cai, S., Cao, Z., Wang, Y., Tang, J., Jalili, R., et al. (2021). Liquid metal enabled continuous flow reactor: A proof-of-concept. Matter *4*, 4022–4041.

32. Majidi, C. (2021). Fluid-like Soft Machines with Liquid Metal. Matter *4*, 336–337.

33. Clarkson, T.W., and Magos, L. (2006). The toxicology of mercury and its chemical compounds. Crit. Rev. Toxicol. *36*, 609–662.

34. Sarigiannis, D.A., Karakitsios, S.P., Antonakopoulou, M.P., and Gotti, A. (2012). Exposure analysis of accidental release of mercury from compact fluorescent lamps (CFLs). Sci. Total Environ. *435–436*, 306–315.

35. Asaduzzaman, A., Riccardi, D., Afaneh, A.T., Cooper, C.J., Smith, J.C., Wang, F., Parks, J.M., and Schreckenbach, G. (2019). Environmental Mercury Chemistry - In Silico. Acc. Chem. Res. *52*, 379–388.

36. Koo, H.J., So, J.H., Dickey, M.D., and Velev, O.D. (2011). Towards all-soft matter circuits: prototypes of quasi-liquid devices with memristor characteristics. Adv. Mater. *23*, 3559–3564.

37. Liu, T., Sen, P., and Kim, C.-J. (2012). Characterization of Nontoxic Liquid-Metal Alloy Galinstan for Applications in Microdevices. J. Microelectromech. Syst. *21*, 443–450.

38. So, J.-H., Koo, H.-J., Dickey, M.D., and Velev, O.D. (2012). Ionic Current Rectification in Soft-Matter Diodes with Liquid-Metal Electrodes. Adv. Funct. Mater. *22*, 625–631.

39. Kazem, N., Hellebrekers, T., and Majidi, C. (2017). Soft Multifunctional Composites and Emulsions with Liquid Metals. Adv. Mater. *29*, 1605985.

40. Lu, Y., Hu, Q., Lin, Y., Pacardo, D.B., Wang, C., Sun, W., Ligler, F.S., Dickey, M.D., and Gu, Z. (2015). Transformable liquid-metal nanomedicine. Nat. Commun. *6*, 10066.

41. Wang, Y., Zhu, C., Pfattner, R., Yan, H., Jin, L., Chen, S., Molina-Lopez, F., Lissel, F., Liu, J., Rabiah, N.I., et al. (2017). A highly stretchable, transparent, and conductive polymer. Sci. Adv. *3*, e1602076.

42. Kim, J.H., Kim, S., So, J.H., Kim, K., and Koo, H.J. (2018). Cytotoxicity of Gallium-Indium Liquid Metal in an Aqueous Environment. ACS Appl. Mater. Interfaces *10*, 17448–17454.

43. Tang, S.-Y., Tabor, C., Kalantar-Zadeh, K., and Dickey, M.D. (2021). Gallium Liquid Metal: The Devil's Elixir. Annu. Rev. Mater. Res. *51*, 381–408.

44. Xu, Y., Su, Y., Xu, X., Arends, B., Zhao, G., Ackerman, D.N., Huang, H., Reid, S.P., Santarpia, J.L., Kim, C., et al. (2023). Porous liquid metal-elastomer composites with high leakage resistance and antimicrobial property for skin-interfaced bioelectronics. Sci. Adv. *9*, eadf0575.

45. Suarez, F., Parekh, D.P., Ladd, C., Vashaee, D., Dickey, M.D., and Öztürk, M.C. (2017). Flexible thermoelectric generator using bulk legs and liquid metal interconnects for wearable electronics. Appl. Energy *202*, 736–745.

46. Markvicka, E.J., Bartlett, M.D., Huang, X., and Majidi, C. (2018). An autonomously electrically self-healing liquid metal-elastomer composite for robust soft-matter robotics and electronics. Nat. Mater. *17*, 618–624.

47. Pan, C., Kumar, K., Li, J., Markvicka, E.J., Herman, P.R., and Majidi, C. (2018). Visually Imperceptible Liquid-Metal Circuits for Transparent, Stretchable Electronics with Direct Laser Writing. Adv. Mater. *30*, e1706937.

48. Malakooti, M.H., Kazem, N., Yan, J., Pan, C., Markvicka, E.J., Matyjaszewski, K., and Majidi, C. (2019). Liquid metal supercooling for low-temperature thermoelectric wearables. Adv. Funct. Mater. *29*, 1906098.

49. Shi, C., Zou, Z., Lei, Z., Zhu, P., Zhang, W., and Xiao, J. (2020). Heterogeneous integration of rigid, soft, and liquid materials for self-healable, recyclable, and reconfigurable wearable electronics. Sci. Adv. *6*, eabd0202.

50. Jang, J., Kim, J., Shin, H., Park, Y.G., Joo, B.J., Seo, H., Won, J.E., Kim, D.W., Lee, C.Y., Kim, H.K., and Park, J.U. (2021). Smart contact lens and transparent heat patch for remote monitoring and therapy of chronic ocular surface inflammation using mobiles. Sci. Adv. *7*, eabf7194.

51. Xu, P., Wang, S., Lin, A., Min, H.K., Zhou, Z., Dou, W., Sun, Y., Huang, X., Tran, H., and Liu, X. (2023). Conductive and elastic bottlebrush elastomers for ultrasoft electronics. Nat. Commun. *14*, 623.

52. Mumcu, G., Dey, A., and Palomo, T. (2013). Frequency-Agile Bandpass Filters Using Liquid Metal Tunable Broadside Coupled Split Ring Resonators. IEEE Microw. Wirel. Compon. Lett. *23*, 187–189.

53. Wang, M., Trlica, C., Khan, M.R., Dickey, M.D., and Adams, J.J. (2015). A reconfigurable liquid metal antenna driven by electrochemically controlled capillarity. J. Appl. Phys. *117*, 194901.

54. Li, S., Bai, H., Liu, Z., Zhang, X., Huang, C., Wiesner, L.W., Silberstein, M., and Shepherd, R.F. (2021). Digital light processing of liquid crystal elastomers for self-sensing artificial muscles. Sci. Adv. *7*, eabg3677.

55. Shu, J., Ge, D.A., Wang, E., Ren, H., Cole, T., Tang, S.Y., Li, X., Zhou, X., Li, R., Jin, H., et al. (2021). A Liquid Metal Artificial Muscle. Adv. Mater. *33*, e2103062.

56. Wissman, J., Dickey, M.D., and Majidi, C. (2017). Field-Controlled Electrical Switch with Liquid Metal. Adv. Sci. *4*, 1700169.

57. Li, X., Tang, S.Y., Li, S., Ge, D., Yang, J., Zhou, J., Yang, H., Zhang, S., Li, W., and Sun, L. (2020). A Robot Boat Powered by Liquid Metal Engines. Adv. Mater. Technol. *6*, 2000840.

58. Mao, G., Drack, M., Karami-Mosammam, M., Wirthl, D., Stockinger, T., Schwödiauer, R., and Kaltenbrunner, M. (2020). Soft electromagnetic actuators. Sci. Adv. *6*, eabc0251.

59. Russell, L., Wissman, J., and Majidi, C. (2017). Liquid metal actuator driven by electrochemical manipulation of surface tension. Appl. Phys. Lett. *111*, 254101.

60. Zavabeti, A., Daeneke, T., Chrimes, A.F., O'Mullane, A.P., Zhen Ou, J., Mitchell, A., Khoshmanesh, K., and Kalantar-Zadeh, K. (2016). Ionic imbalance induced self-propulsion of liquid metals. Nat. Commun. *7*, 12402.

61. Wang, E., Shu, J., Jin, H., Tao, Z., Xie, J., Tang, S.Y., Li, X., Li, W., Dickey, M.D., and Zhang, S. (2021). Liquid metal motor. iScience *24*, 101911.